Journal of Basic Physical Research ISSN: 2141-8403 Prints, 2141-8411 Online
Vol.14, Issue 2, October, 2025, pp. 100 – 123, Available online at https://journals.unizik.edu.ng/jbpr/

HYDROCARBON POTENTIAL ASSESSMENT OF OLUS FIELD THROUGH INTEGRATED PETROPHYSICAL AND SEISMIC CHARACTERIZATION OF CRETACEOUS-TERTIARY RESERVOIRS, CALABAR FLANK, LOWER BENUE TROUGH, NIGERIA.

Bankole, Olusegun Olayinka[1], Jimoh Ajadi[1] and *Gabriel Efomeh Omolaiye[2]
[1]*Department of Geology and Mineral Science, Kwara State University, Malete, Kwara State, Nigeria*
[2]*Department of Applied Geophysics, University of Ilorin, PMB 1515, Ilorin, Kwara State, Nigeria*

Abstract
As frontier exploration expands, the Calabar Flank remains underexplored due to the lack of detailed quantitative reservoir evaluation in the south-eastern part of Nigeria, despite the promising geological conditions of the region for hydrocarbon accumulations. This study assesses the hydrocarbon potential of the OLUS Field in Calabar Flank by integrating petrophysical analysis, seismic interpretation, volumetric estimation and depositional environment. Petrophysical evaluation reveals high-quality reservoirs with net-to-gross ratios of 0.81-0.95, porosity up to 0.37, favourable hydrocarbon saturations, and low bulk volume water, indicating laterally continuous pay zones. Seismic evaluation identifies fault-bounded closures and rollover anticline structures. The assessment of direct hydrocarbon indication and the amplitude conformity with structures further gives credibility to the presence of hydrocarbon within the exploration areas. Volumetric estimates show substantial un-risked STOIIP with deep-level leads of OLUS South and OLUS East dominating due to large GRVs despite lower reservoir quality. At the same time, mid-level prospects of OLUS North and OLUS East offer lower-risk targets. Depositional analysis indicates a Cretaceous transgressive sequence from fluvial-deltaic to shallow marine carbonates and open marine shales, controlled by sea-level fluctuations and tectonics. The integrated results highlight multiple play types with varying risk and scale, providing a framework for prioritizing exploration targets and guiding field development.

Keywords: *Calabar Flank, Seismic Characterization, Petrophysical Analysis, Hydrocarbon Assessments.*

Introduction
The evaluation of hydrocarbon potential has evolved significantly with the integration of advanced petrophysical techniques and seismic interpretation to enable more accurate subsurface characterization (Ekop et al., 2025; Falade et al., 2024; Onita et al., 2023). In Nigeria, the pursuit of sustainable energy has heightened the importance of maximizing hydrocarbon resource identification and recovery, particularly from underexplored fields with proven petroleum systems like the Calabar Flank, with growing interest in its stratigraphic and structural settings (Aka et al., 2022; Ekwok et al., 2021; Ogidi et al., 2021). The Calabar Flank is structurally bounded by a transitional zone between continental and marginal marine environments that features sequences associated with multiple phases of tectonic activity and sediment accumulation (Selema et al., 2023). Understanding the distribution, geometry, and quality of these reservoirs is essential for hydrocarbon prospectivity. Previous studies have provided regional insights into the stratigraphy and structure of the Calabar Flank. However, field-specific analysis that integrates well log data, seismic profiles, and petrophysical parameters is sparse, particularly for the OLUS Field (Harry et al., 2022).

In hydrocarbon exploration, petrophysical analysis offers direct insights into critical rock and fluid properties that estimate reservoir capacity and production potential (Ekop et al., 2025; Mheluka et al., 2018). By analysing well logs and core data, this study examines the quality of reservoirs within the OLUS Field to identify productive zones and delineate fluid-bearing formations. Additionally, integrating seismic data with petrophysical analysis enables cross-validation of subsurface interpretations, reducing uncertainties and increasing confidence in characterizing reservoir units. Moreover, seismic interpretation provides the necessary information to support petrophysical insights, where key structural elements are mapped and

integrated with petrophysical data to build a coherent reservoir study through the analysis of seismic datasets (Onita et al., 2023; Oyeyemi et al., 2017). Seismic attributes are interpreted alongside petrophysical parameters to infer lithology, depositional patterns, and potential fluid distributions (Falade et al., 2024; Khan et al., 2024). This integrative approach identifies potential hydrocarbon zones and highlights the depositional controls and structural factors that influence reservoir distribution, while allowing for the delineation of structural traps and stratigraphic pinch-outs in the OLUS Field located in the Calabar Flank region (Ahmad et al., 2021).

This study assesses the OLUS Field's hydrocarbon potential by utilizing both petrophysical analysis and seismic interpretation. It aims to enhance understanding of the field's reservoir and provide valuable insights into the broader hydrocarbon prospects of the Calabar Flank to support more effective exploration and development strategies in the region.

Geological setting of Calabar Flank

The Calabar Flank is located geographically between latitude 5°0'0"N and 5°15'0"N, and longitude 8°15'0"E and 8°30'0"E. It was identified by Murat in 1972 as one of the sedimentary basins in southern Nigeria characterized by crustal blocking faults with formation linked to early rifting events during the Albian stage (Ekwok et al., 2021; Boboye et al., 2014; Ekpo et al., 2013; Okiwelu et al., 2010; Murat, 1972). It is bounded by the Oban Massif, the Calabar Hinge, the Ikpe Platform and the Cameroon Volcanic Line as illustrated in Figure 1 (Ekwok et al., 2021; Petters et al., 1995). Calabar Flank have a well-defined sedimentary succession consisting of eight major formations arranged sequentially from the base to the top (Essien et al., 2005; Edet & Nyong, 1993; Petters et al., 1995). These formations are the Awi Formation, Mfamosing, Ekenkpon Shale, New Netim Marl, Nkporo Shale, Imo Shale, Ameki, and the Benin Formation, as shown in Figure 2 (Aka et al., 2022; Ekwok et al., 2021; Boboye et al., 2014; Odumodu, 2012; Petters, 1982).

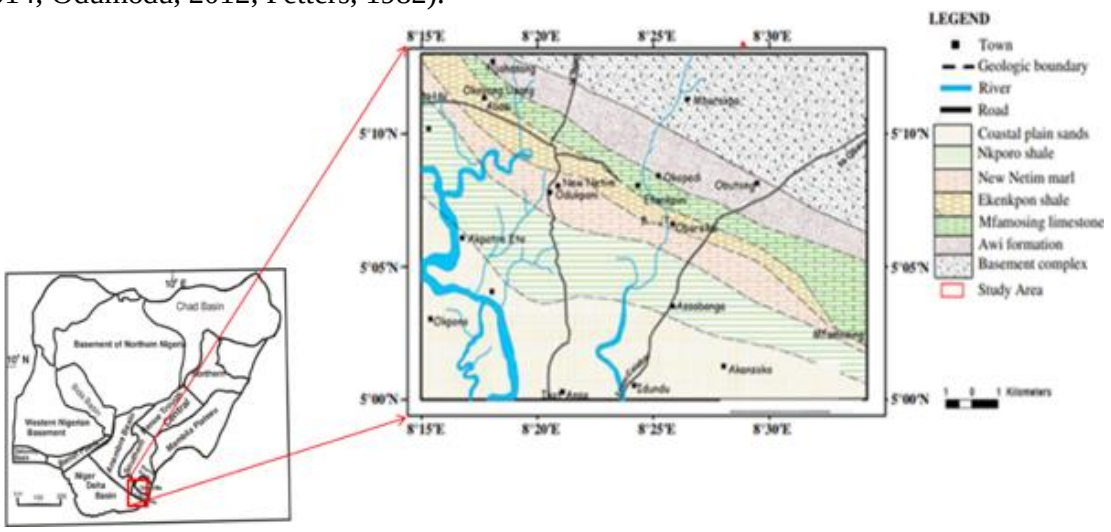

Figure 1: Geologic Map showing Calabar Flank Modified after Ekwok et al. (2021)

The Awi formation begins the sedimentation within Calabar Flank as the oldest deposit, dated to Aptian age, lies unconformably over the Precambrian Basement Complex, and it is predominantly made up of fluvio-deltaic sediments, as shown in Figure 3 (Aka et al., 2022; Ukpong et al., 2017; Boboye et al., 2014; Ekpo et al., 2013; Ramanathan & Kumaran, 1981; Adeleye & Fayose, 1978). Petrographic analysis indicates that the sedimentary components of the Awi Formation were sourced from a mixture of acidic igneous rocks, granitic pegmatite, and metamorphic rocks derived from the southwestern Nigerian basement terrain (Okon &

Ojong, 2019). Overlying the Awi Formation is the carbonate-rich Mfamosing Formation, dated to the Middle Albian based on the presence of ammonite fossils (Reijers, 1998; Reijers & Petters, 1987). The Mfamosing carbonates were deposited before the regional tectonic event marked by compressional tectonics, basic volcanic activity, and stratigraphic disconformities that influenced subsequent deposition across the Calabar Flank (Reijers et al., 1998; Petters et al., 1995). Together, Awi and Mfamosing units constitute part of the Odukpani Group.

TERTIARY	AGE	FORMATION	LITHOSTRATIGRAPHIC DESCRIPTION	DEPOSITIONAL
	OLIGOCENE TO RECENT	Benin Formation	Pebbly sands and gravels	Continental
	EOCENE	Ameke Formation	Medium-grained pebbly sandstones, clayey sandstones, calcareous silts, clay and thin limestones	Paralic
	PALEOCENE	Imo Shale	Clayey shale, clay ironstones bands, thin sandstone and sandy limestone bands	Paralic
CRETACEOUS	MAASTRICHTIAN	Nkporo Shale	Gypsiferous dark grey shales with ironstone intercalation	Shallow Marine
	CAMPANIAN		Uncomformity	
	SANTONIAN	New Netim Marl	Marlstones with shale intercalations	Marine
	CONIACIAN			
	TURONIAN	Ekenkpon Shale	Thick black pyritic shales with intercalations of mudstones, sandstones, ironstones and oyster beds	Marine
	CENOMANIAN			
	ALBAIN	Mfamosing	Stromatollitic fossiliferous limestones	Marine
	APTIAN	Awi Formation	Arkosic sandstones interbedded with shales	Fluvio – deltaic
	PRECAMBRIAN	Oban Basement	Crystalline Basement Rocks	

Figure 2: Stratigraphic Sequence of Calabar Flank (Odumodu, 2012)

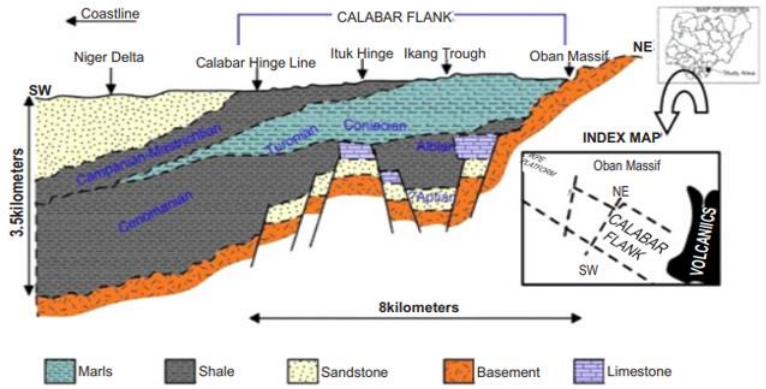

Figure 3: Geological Cross-section of Calabar Flank displaying Structural Element and Conceptual Subsurface Sequence (Nyong & Ramathan, 1985)

After the Mfamosing Formation, the Ekenkpon Shale Formation was laid down, which began a significant marine transgressive phase that began in the Late Albian and extended into the Turonian, with a brief regression occurring during the Cenomanian (Nton et al., 2018; Ilori, 2016; Nyong & Ramanathan, 1985). The Ekenkpon Shale is mainly composed of dark, fissile shales interlayered with calcareous mudstones, marls, and occasional shell-rich beds, and the depositional characteristics of the Ekenkpon Shale reflect the influence of two key transgressive events, both of which are stratigraphically linked to the more extensive Nkalagu Formation (Oluwajana & Ehinola, 2018). Subsequently, the New Netim Marl Formation was deposited and characterized by thick marl beds interlayered with thinner shale seams dated to the Coniacian stage, which preceded the formation of the New Netim Marl (Ilori, 2016). Furthermore, above the Ekenkpon Shale Formation lies the Nkporo Shale Formation, composed of dark grey to bluish-black carbonaceous shales that are typically friable to flaggy (Ogidi et al., 2021; Harry et al., 2022). This formation also includes interbeds of marly, silty, and sandy shales as well as mudstones and is assigned to the Campanian-Maastrichtian timeframe (Ogidi et al., 2021).

Moreover, depositional activity continued with the overlaying Imo Shale, Ameki Formation, and Benin Formations (Harry et al., 2022). The Imo Shale Formation reflects a post-Cretaceous depositional environment that transitioned into a regressive sequence, composed of bluish-grey clays and black shale, interspersed with calcareous sandstone bands, marl, and limestone lenses (Udo et al., 2023). The Ameki Formation overlies the Imo Shale and formed during the early Eocene. Throughout the middle to late Eocene, this unit experienced an increase in sand content, indicating the onset of regional regression and the development of deltaic environments within the Calabar Flank (Udo et al., 2023). The Benin Formation represents the most recent stratigraphic unit in the area, spanning from the Miocene to the present. It is primarily made up of unconsolidated sands with minor clay components (d'Almeida et al., 2016).

Materials and Methods

The dataset used in this study comprises four well logs, a 156 km² 3D seismic cube, one checkshot, and three deviation survey data sets acquired within the study area. The well log data consist of gamma ray (GR), spontaneous potential (SP), resistivity, density, and sonic logs, which provide essential information for lithological identification, fluid type discrimination, porosity evaluation, and saturation estimation. Techlog software was used for advanced calibration of the well logs. Figures 4 show the base map and the log correlation panel of OLUS Field, respectively.

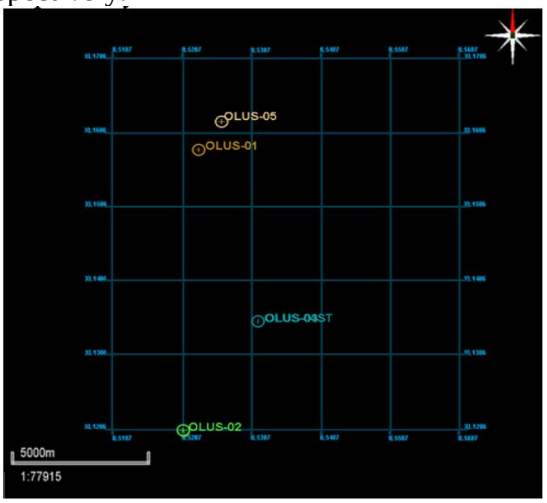

Figure 4: Base map of the Well Log in the OLUS field within the study area

Petrophysical Data Analysis

The Petrophysical analysis involved a systematic workflow to evaluate reservoir properties and hydrocarbon potential within the OLUS Field. The procedure followed a structured workflow:

Gross Rock Volume (GRV): This represents the total volume of rock within a defined reservoir structure that lies above the hydrocarbon-water contact, as shown using this formula in Equation 1.

$$\boldsymbol{GRV = A * h} \qquad \textbf{Eqn. 1}$$

Where **A** is the areal extent of the reservoir, and **h** is the gross thickness of the reservoir.

Shale Volume Estimation (Vsh): utilizing the linear Gamma Ray Index method to quantify the volume of shale within the reservoir as shown in equations 2 and 3 (Omigie & Alaminiokuma, 2020).

$$\boldsymbol{GR_{index} = \frac{GR - GR_{matrix}}{GR_{shale} - GR_{matrix}}} \qquad \textbf{Eqn. 2}$$

$$\boldsymbol{V_{sh} = 0.083 * (2^{(3.7 * GR_{index})} - 1)} \qquad \textbf{Eqn. 3}$$

Where the Gamma-ray log reading within the zone of interest ($\boldsymbol{GR}$); Gamma-ray log reading in 100% matrix rock ($\boldsymbol{GR_{matrix}}$); Gamma-ray log reading in 100% shale ($\boldsymbol{GR_{shale}}$); Gamma-ray index ($\boldsymbol{GR_{index}}$) and volume of shale ($\boldsymbol{V_{sh}}$)

Porosity Estimation (Ø): Porosity represents the fraction of the rock volume that is occupied by pore spaces, which can store fluids such as hydrocarbons or water (Nwaezeapu et al., 2019; Saadu & Nwankwo, 2018). In clean formations, porosity is typically estimated using the density log method using equation 4 below.

$$\boldsymbol{Ø_D = \frac{(\rho_{ma} - \rho_b)}{(\rho_{ma} - \rho_{fluid})}} \qquad \textbf{Eqn. 4}$$

Where $Ø_D$ is the total porosity; $\boldsymbol{\rho_{ma}}$ is the density of the rock matrix; $\boldsymbol{\rho_b}$ is the bulk density read from the log and $\boldsymbol{\rho_{fluid}}$ is the density of the fluid occupying the pore spaces.

Water Saturation ($\boldsymbol{S_w}$): This is the proportion of the pore space in a reservoir that is filled with water, which is a critical factor in estimating hydrocarbon-in-place and can be calculated using Archie's equation in equation 5 below for clean formation (Nwaezeapu et al., 2019; Oyeyemi et al., 2017). Moreover, Pickett plot analysis was employed to estimate water saturation and assess hydrocarbon potential by integrating resistivity and porosity data from well logs.

$$\boldsymbol{S_w = \sqrt[n]{\frac{a * (\frac{Ø^m * R_0}{a})}{R_t * Ø^m}}} \qquad \textbf{Eqn. 6}$$

Where **a** is the tortuosity factor, **m** is the cementation exponent; Ø is porosity; $\boldsymbol{R_0}$ is the resistivity of the reservoir when the entire fluid is water, $\boldsymbol{R_t}$ is the true resistivity, and **n** is the saturation exponent.

Hydrocarbon Saturation ($\boldsymbol{S_h}$)

This is the portion of the pore space occupied by hydrocarbons and is obtained by subtracting water saturation from unity, as shown in equation 7 (Nwaezeapu et al., 2019). Where $\boldsymbol{S_w}$ is Water Saturation.

$$\boldsymbol{S_h = 1 - S_w} \qquad \textbf{Eqn. 7}$$

Net-to-Gross Ratio (NTG): The net-to-gross ratio (NTG) is the proportion of net reservoir to the total gross interval using equation 8 (Nwaezeapu et al., 2019).

$$NTG = \frac{Net\ Reservior\ Thickness}{Total\ Formation\ Thickness} \quad \textbf{Eqn. 8}$$

Bulk Volume Water (BVW): This represents the fraction of the total rock volume that is occupied by formation water, using equation 9 below (Oyeyemi et al., 2017; Al-Baldawi, 2014).

$$\boldsymbol{BVW = \emptyset * S_w} \quad \textbf{Eqn. 9}$$

Where Ø Is porosity and $\mathbf{S_w}$ is Water Saturation

Formation Volume Factor (B_o): The formation volume factor (B_o) is the ratio of the volume of oil at reservoir conditions to the volume at surface (stock tank) conditions surface using equation 10 below (Hussein et al., 2024).

$$\boldsymbol{B_o = \frac{Volume\ at\ Reservior\ Conditions}{Volume\ at\ Surface\ Conditions}} \quad \textbf{Eqn. 10}$$

Seismic Interpretation

Seismic data interpretation involved detailed horizon picking and fault delineation from the 3D seismic volume to accurately define key stratigraphic and structural features that influence reservoir geometry. Time-to-depth conversion was achieved using well-derived velocity models. Moreover, Reservoir volumes were then estimated using the volumetric method, integrating results from 3D seismic interpretation and petrophysical data analysis. Depth structural contour maps of the productive reservoir horizons were generated by converting interpreted seismic times at key stratigraphic tops into depth using average interval velocities. The original hydrocarbons in place (OHIP) are discussed below.

Original Oil in Place (OOIP): This is the total volume of oil originally present in the reservoir, regardless of its recoverability using equation 11 (Paul et al., 2018).

$$\boldsymbol{OOIP = \frac{7758 \times A \times h \times \emptyset \times (1 - S_w)}{B_o}} \quad \textbf{Eqn. 11}$$

Where A is Area in acres; h is net pay thickness in feet; Ø is porosity; S_w is water saturation; B_o is formation volume factor in bbl/STB; and 7758 is a conversion factor from acre-feet to barrels.

Stock Task Oil Initially in Place (STOIIP): This is the volume of oil originally in place, adjusted to surface (stock tank) conditions, same as OOIP but expressed at standard conditions (Saadu & Nwankwo, 2018). The STOIIP can be grouped into unrisked and risked STOIIP.

The Unrisked STOIIP represents the full volume of oil initially in place estimated in a prospect, assuming full geological success. While Risked STOIIP is the volume of oil in place adjusted for geological or commercial risk (Cook, 2021). It represents the expected value by factoring in the probability of success, where Risked STOIIP is equal to the multiple of Unrisked STOIIP and Probability of Success (Cook, 2021). In addition, Probability of Success (POS) is a metric used to estimate the likelihood that a prospect contains recoverable hydrocarbons. POS is simply equal to the multiple of trap, source, migration, and reservoir quality (Cook, 2021). Each component is assigned a probability between 0 and 1, and the product gives the overall POS.

Results
Petrophysical Analysis
Well OLUS-03 of Sand A

The petrophysical interpretation of the reservoir zone in Well OLUS-03 targeting Sand A shows strong reservoir integrity and promising hydrocarbon saturation, as detailed in Tables 1 and 2 below. The gross interval measures 43.11 ft with a net sand thickness of 34.92 ft, indicating the dominance of clean, reservoir-quality sandstone. As shown in Figure 5 below, the volume of shale content across the interval is minimal, while Figure 6 shows a picket plot used in determining water saturation. Both gross and net pay match the gross and net sand measurements, suggesting the entire sand interval is hydrocarbon-bearing and meets the established pay criteria. The calculated net-to-gross (NTG) ratio of 0.81 further supports high reservoir quality and lateral continuity of the sand body. The average porosity is 0.37, signifying excellent pore connectivity and adequate space for hydrocarbons. Water saturation (Sw) is calculated at 0.45 while hydrocarbon saturation (Sh) reaches 0.55, confirming hydrocarbons occupy a significant portion of the pore system. The bulk volume of water (BVW) is relatively low at 0.167, indicating minimal irreducible water. Collectively, these attributes define an oil-down-to (ODT) system.

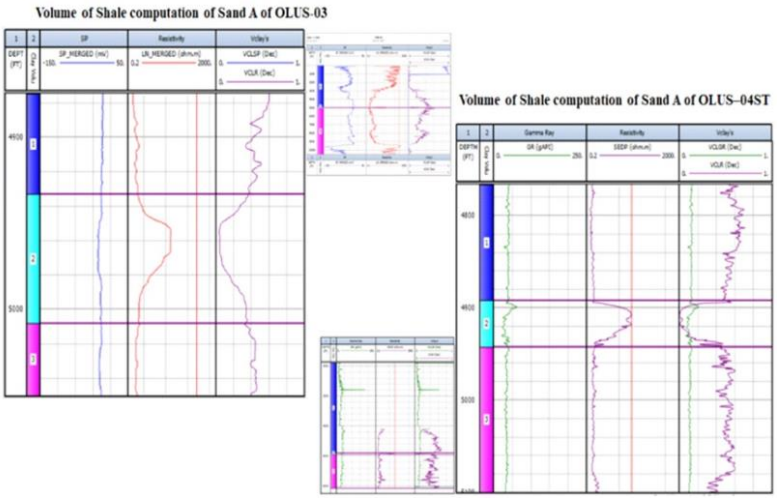

Figure 5: Volume of shale computation of Sand A within OLUS–03 and OLUS–04ST

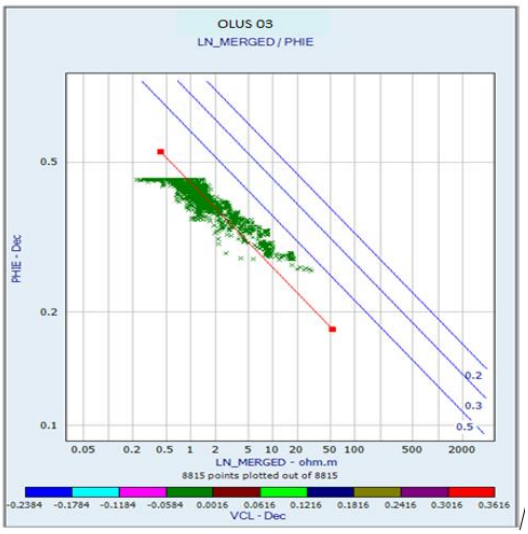

Figure 6: Pickett plot used in the determination of water saturation in OLUS-03 well

Well OLUS-03 of Sand B

Table 2 shows that OLUS-03 targeting Sand B demonstrates outstanding reservoir quality with exceptionally high hydrocarbon saturation. As shown in Figure 7 displaying the reservoir from the OLUS-03 well, both the gross and net sand thicknesses are notably extensive, measuring 879 ft and 835 ft, respectively. The NTG ratio is remarkably high at 0.95, indicating minimal shale content and higher sand continuity. Petrophysical measurements reveal the average water saturation (Sw) of only 0.09, which is a high hydrocarbon saturation (Sh) of 0.91, signifying that the pore spaces are predominantly filled with hydrocarbons. Additionally, the bulk volume of water (BVW) is very low at 0.0225, highlighting limited irreducible water and effective hydrocarbon displacement. These parameters collectively support the classification of this reservoir as a high-grade oil-down-to (ODT) system.

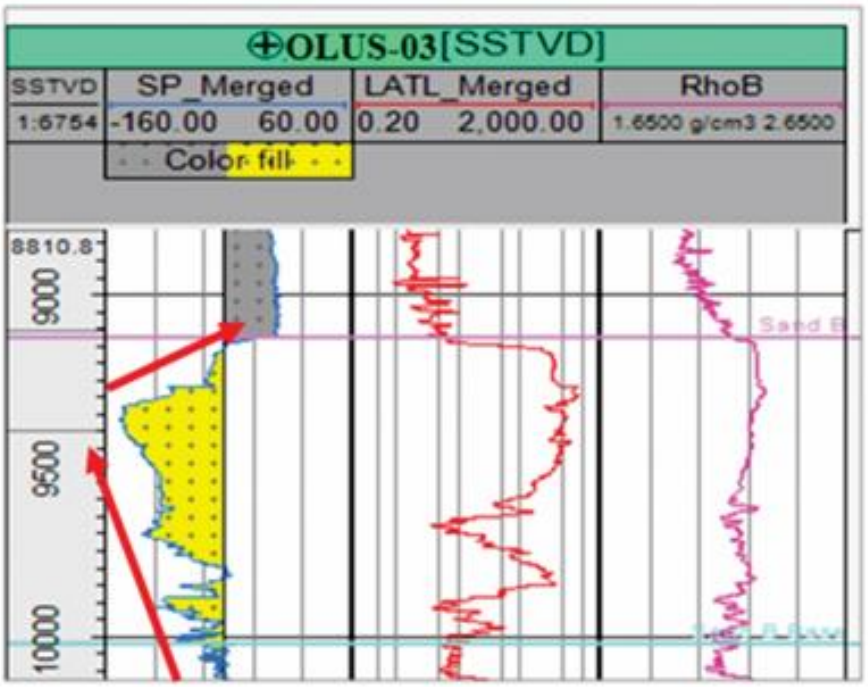

Figure 7: showing one of the reservoirs from OLUS-03 Well

Well OLUS-04ST

The analysis of petrophysical parameters in Well OLUS-04ST within the Sand A interval reveals excellent reservoir characteristics with strong hydrocarbon potential, as shown in Table 2 below. Figures 8 and 9 display the shale volume estimation and Pickett plot used to get the water saturation of Sand B, respectively. The gross sand thickness is 48.45 ft, while the net pay sand is 42.15 ft, indicating a fully productive reservoir section with minimal non-reservoir intervals, as shown in Table 2. This strong correlation indicates the presence of a laterally continuous and clean sandstone unit. A high net-to-gross (NTG) ratio of 0.87 demonstrates consistent sand development and a robust reservoir framework. The porosity values indicate an adequate pore space for fluid accumulation, with a water saturation (Sw) of 0.52 and a hydrocarbon saturation (Sh) of 0.48. These figures reflect a moderately saturated hydrocarbon-bearing system. The reservoir is further classified as an oil-down-to (ODT) contact, indicating the presence of hydrocarbons throughout the entire pay section.

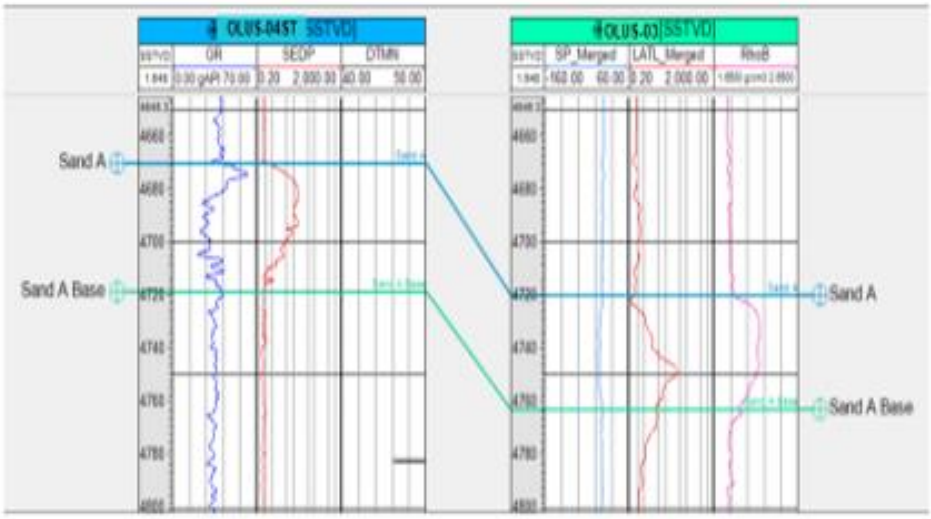

Figure 8: Well Correlation between Sand A as seen in both OLUS-04ST and OLUS-03 Wells

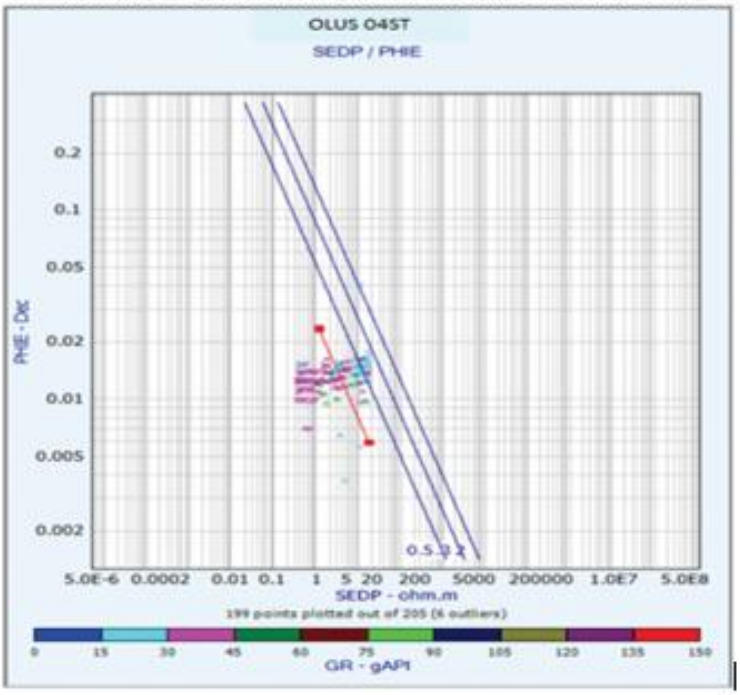

Figure 9: Pickett plot used in the determination of water saturation in OLUS-04ST well

Table 1: Top and Base Properties Across the Wells within OLUS Field

WELLS	SANDS	TOP MD (ft)	TVDSS (ft)	BASE MD (ft)	TVDSS (ft)
OLUS–03	**Sand A**	4942.54	-4719.94	4985.69	-4763.05
OLUS-04ST	**Sand A**	4894.80	-4670.14	4944.24	-4718.59
OLUS-03	**Sand B**	9364.84	9140.8	10244.0	10019.8

Table 2: Petrophysical Well Logs Properties across the Wells within OLUS Field

WELLS	GROSS SAND (ft)	NET SAND	GROSS PAY	NET PAY	POROSITY	WATER SATURATION	NTG	REMARKS
OLUS–03	43.11	34.92	43.11	34.92	0.37	0.45	0.81	ODT
OLUS-04ST	48.45	42.15	48.45	42.15	*---	0.52	0.87	ODT
OLUS-03	879	835	879	835	0.25	0.09	0.95	ODT

(ODT – oil-down-to system)

Seismic Interpretation

Figure 10 shows an uninterpreted and interpreted seismic section. In the interpreted section, faults were mapped and annotated, revealing a predominantly extensional structural regime with both synthetic and antithetic splays that compartmentalise the succession. Fault geometries are segmented with ramps and transfer zones rather than single, planar displacements, indicating stepped displacement and potential fault-tip closures at reservoir levels. The fault throw increases downward across the section, implying growth fault behaviour. Several faults cut through multiple horizons, suggesting they are basin-scale features that influence migration pathways and trap integrity. These mapped faults define a mix of structural traps, such as fault-bounded closures and fault-tip anticlines, as well as potential migration barriers. This information is important for prospect risk ranking and for linking petrophysical well data to seismic horizons.

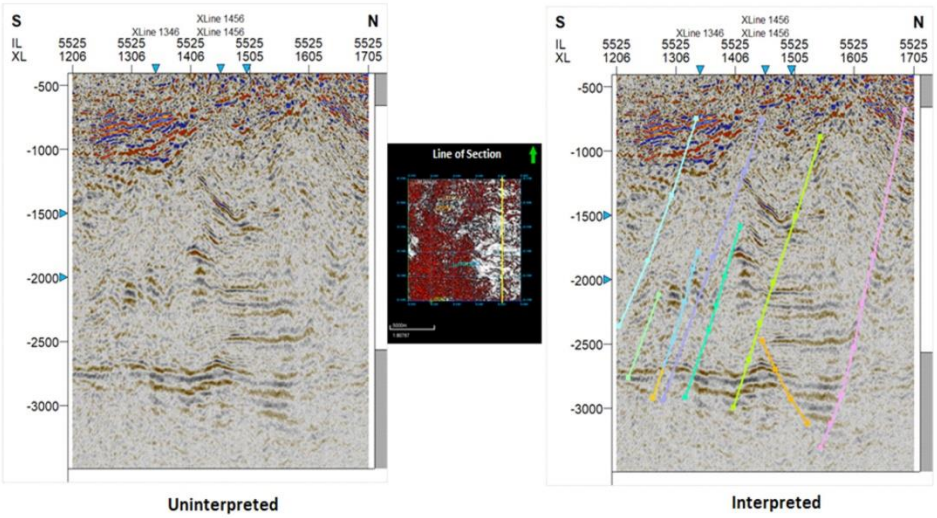

Figure 10: An uninterpreted and interpreted seismic section with fault interpretation

In addition, Figure 11 shows an inline 5300 and crossline 1350 seismic section, which the inline displays lateral continuity of key reflectors and highlights vertical displacement and reflector terminations against mapped faults for assessing along-strike continuity of prospective intervals and for correlating bright spots or amplitude anomalies with structural relief. The cross-line XL 1350 complements that by showing dip-direction behaviour, where reflector curvature and onlap patterns reveal subtle drape over structural highs and possible fault-bend folds. Together, these orthogonal sections allow confident identification of both closed structural geometries like local anticlinal shoals and fault-

bounded highs. and stratigraphic variations. Additionally, the top of reservoirs A and B is interpreted on inline 5300 and crossline 1350, as shown in Figure 11. However, there are seismically transparent reflections between the two mapped surfaces, which is typical of shale, and some bright spots encased within the seismic reflective zones.

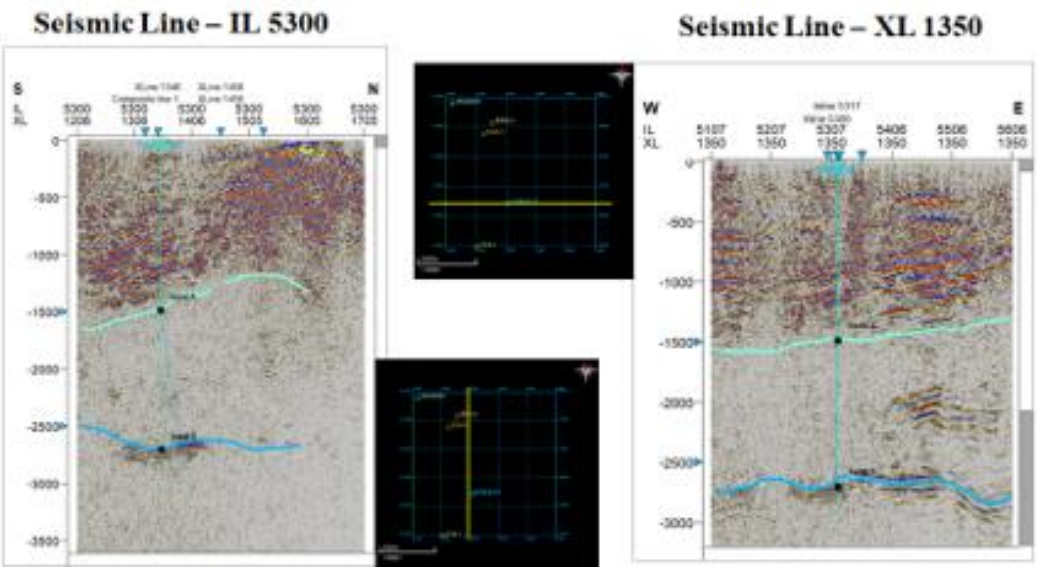

Figure 11: Inline 5300 and crossline 1350 of the study area

The Velocity Model plot is shown in Figure 12, while Figures 13 and 14 display the time map and depth map of Sand A and B. The time map shows contours of two-way travel time that define structural highs and lows across the study area. Closed positive anomalies on the time map indicate potential structural closures. When converted to depth, the depth map retains these closures but also reveals variations caused by the velocity model, where areas that appear modest in time can become more pronounced in depth, depending on local velocity trends.

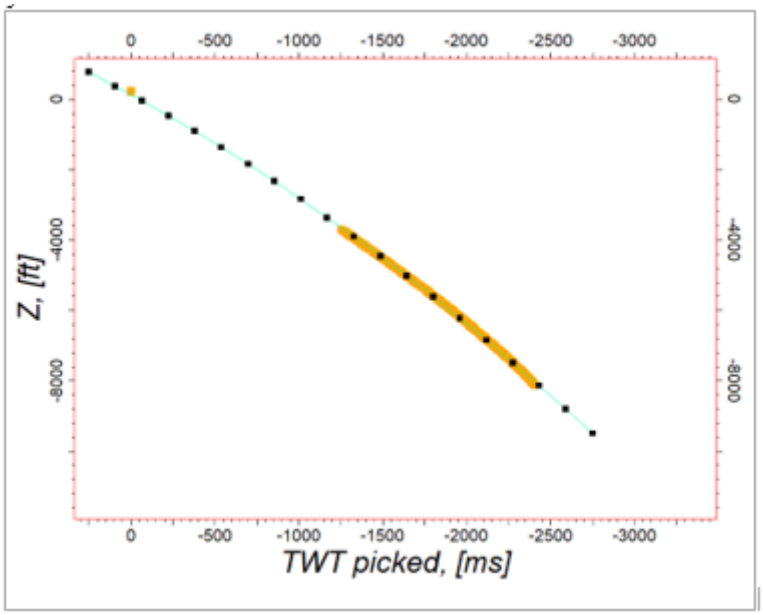

Figure 12: Velocity Model (Time-Depth) Plot

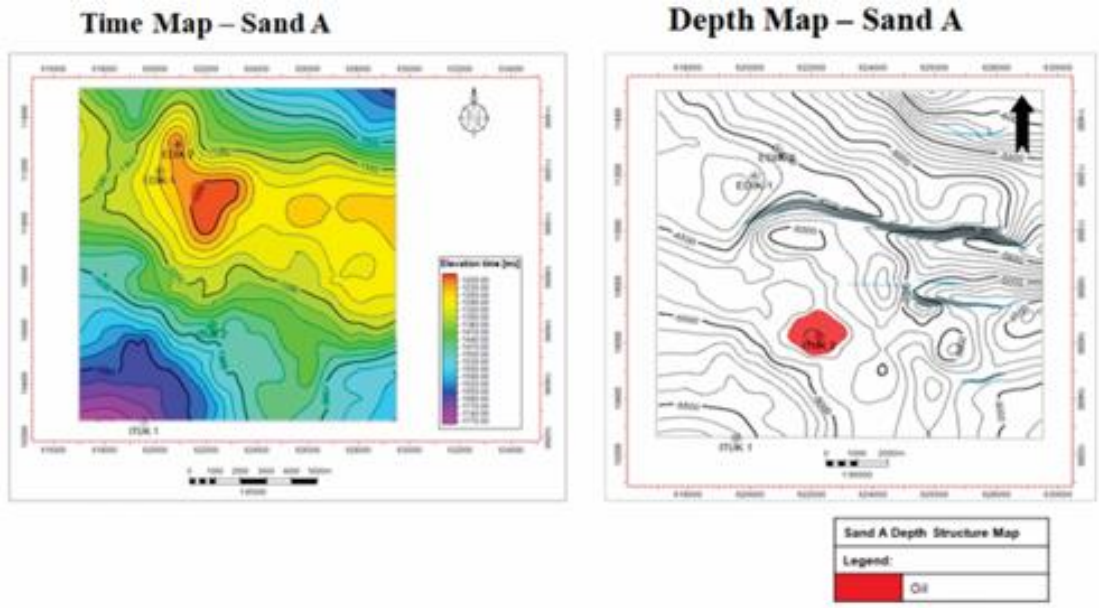

Figure 13: Time and Depth maps of Sand A

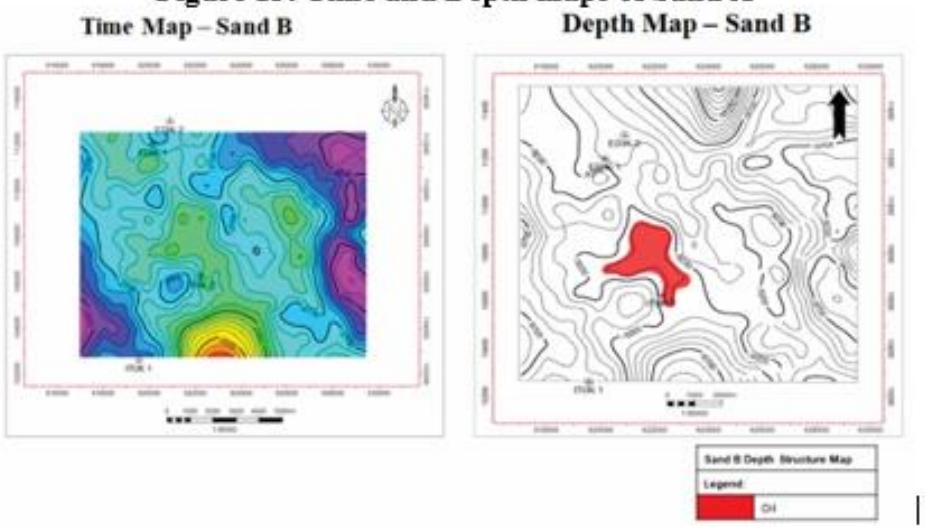

Figure 14: Time and Depth maps of Sand B

Resources Estimation

Table 3 shows the evaluated volume of hydrocarbon in Sand A and B, indicating potential distribution in the two sand units.

Table 3: Volume Estimation of Hydrocarbon in Sand

Reservoirs	**GRV**	**Area**	**NTG**	**Sw**	**Φ**	**OOIP**	**Bo**	**STOOIP**	**RF**	**EUR**
	Acre-ft	Acre	frac	frac	frac	MMBO		MMBO		MMBO
Discovery										
Sand A	18,197	**	0.81	0.45	0.37	23.27	1.15	20.23	0.3	6.07
Sand B	208,583	**	0.95	0.09	0.25	349.73	1.15	304.11	0.3	91.23
Total								**324.35**		**97.30**

Furthermore, the identified opportunities on crossline 1450 and Inline 5485, as shown in Figure 15, and crossline 1450 and inline 5485 in Figure 16, are geologic features that are typical of direct hydrocarbon indicators (DHI): a bright spot encased within seismically transparent reflectors. The top and base of these opportunities were mapped across the entire seismic volume, showing Figures 15 and 16. The time and depth structure maps were generated for each of the levels to evaluate the opportunities that revealed that both opportunities are fault-dependent closures, displayed in Figures 17 - 22. The RMS amplitude generated over the surfaces shows that they are amplitude-supported, as shown in Figures 17 – 22. Figure 23 shows the prospect and lead map for visualizing identified potential hydrocarbon-bearing structures and stratigraphic traps within the Calabar Flank. The combination of potential prospects and emerging leads underscores a diverse petroleum system with multiple play types and varying levels of risk, offering opportunities for phased exploration, portfolio management, and future field development.

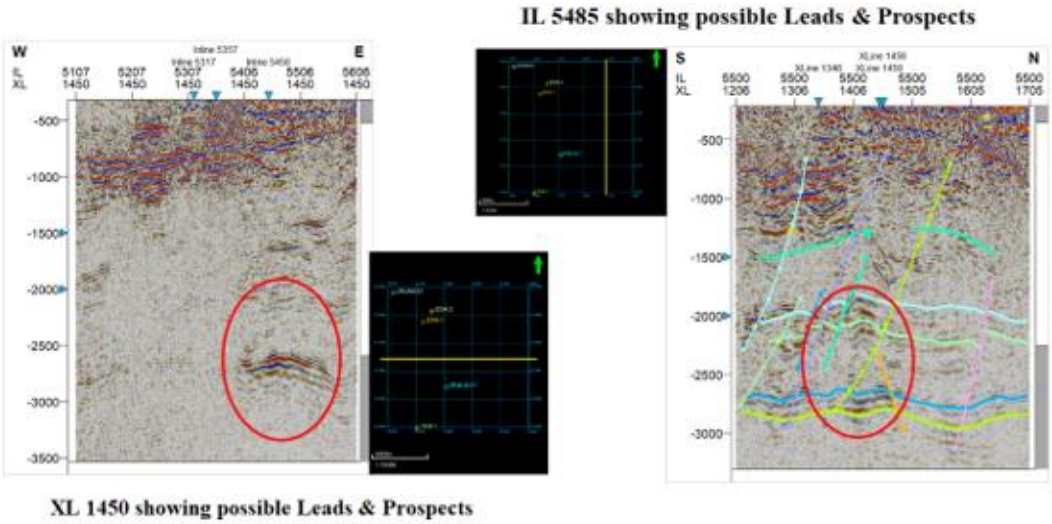

Figure 15: Possible Lead and Prospects at XL1450 and IL 5485 of the study area

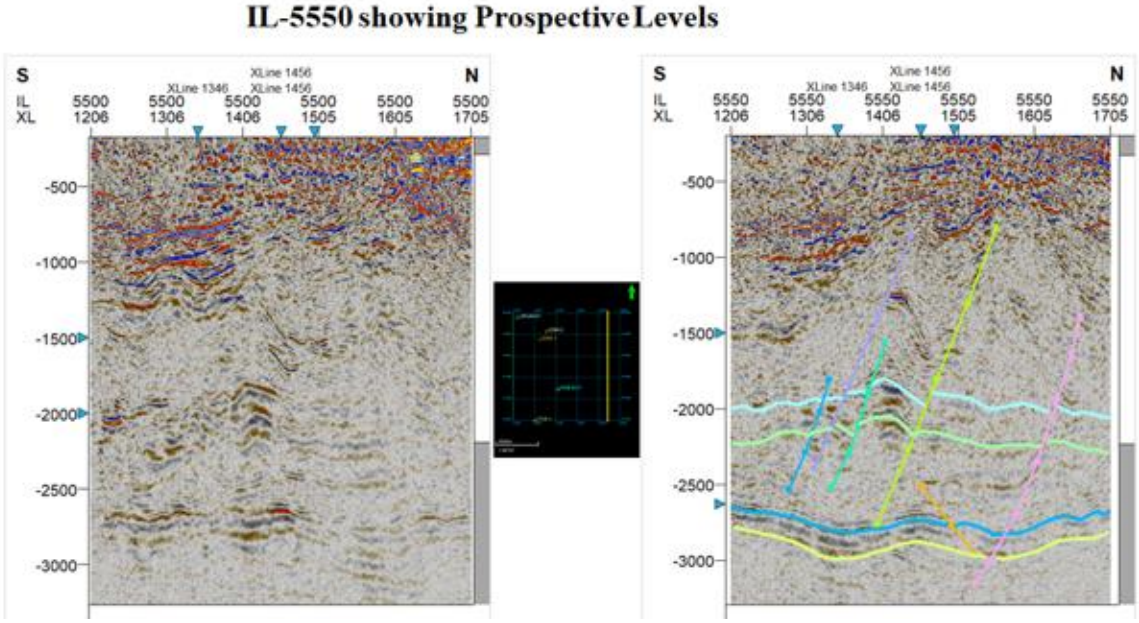

Figure 16: Possible Lead and Prospects at IL 5550 of the study area

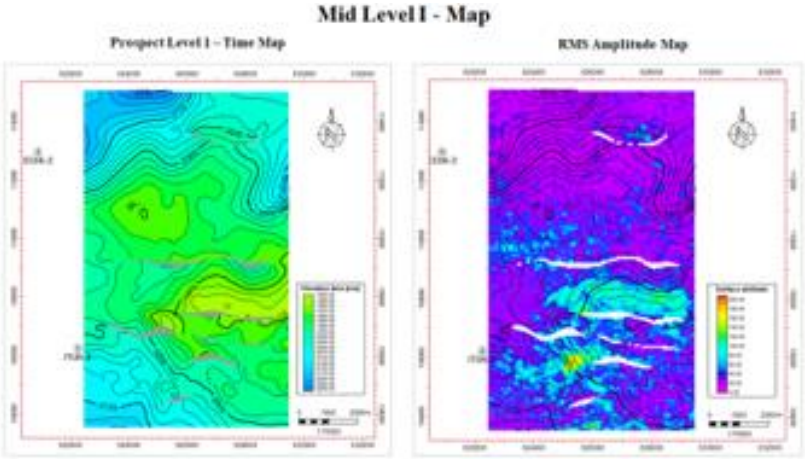

Figure 17: Mid-Level I time map for Prospect Level 1 and RMS Amplitude Map

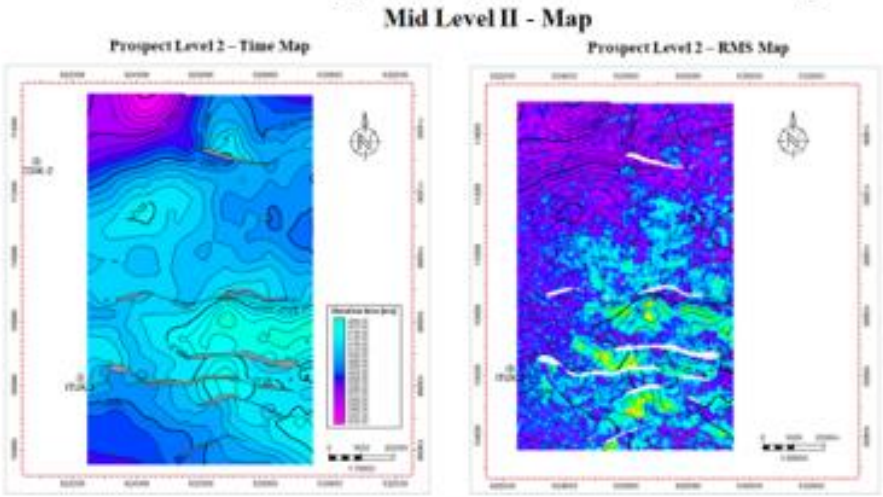

Figure 18: Mid-Level II time map for Prospect Level 1 and RMS Amplitude Map

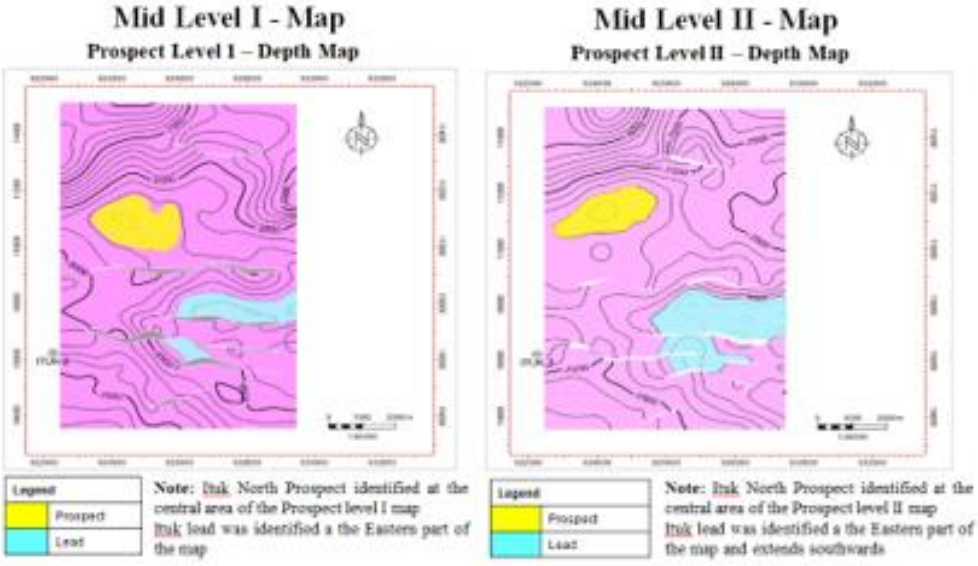

Figure 19: Mid-Level I Depth map for Prospect Level I and II

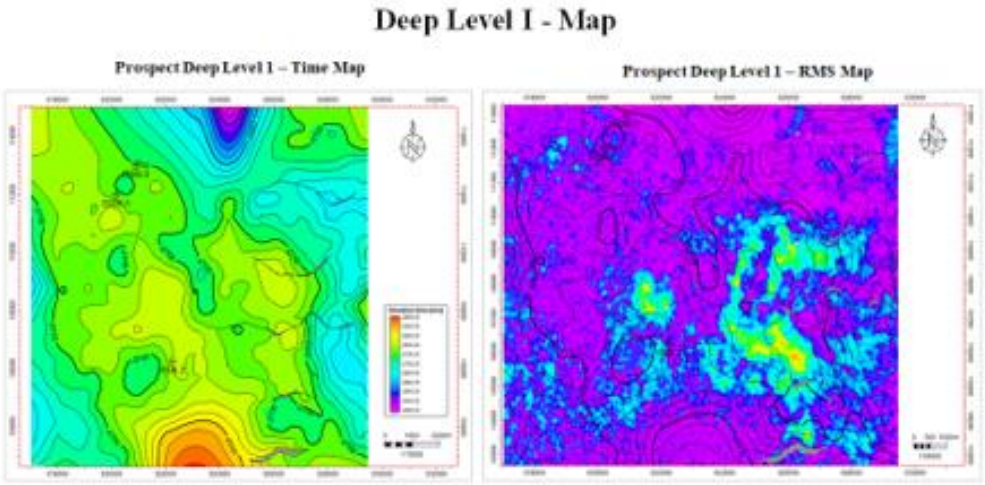

Figure 20: Deep-Level I time map for Prospect and RMS Amplitude Map for Level I

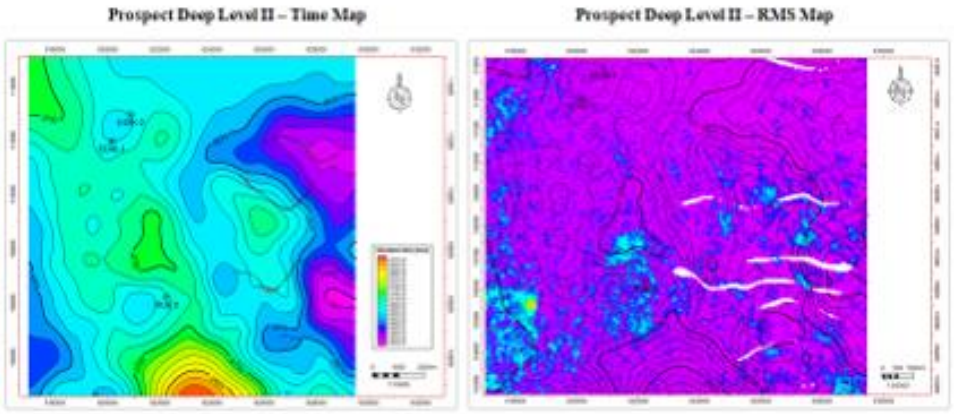

Figure 21: Deep-Level II-time map for Prospect and RMS Amplitude Map for Level II

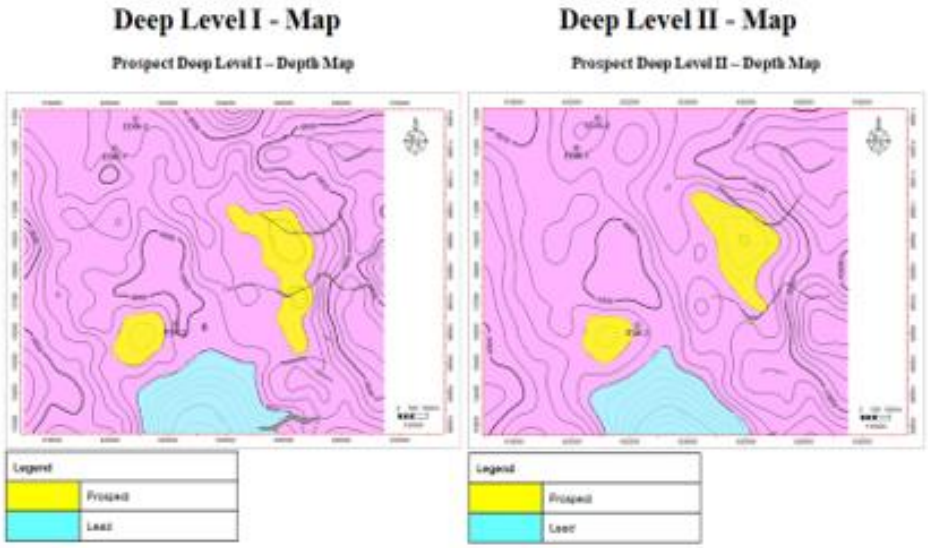

Figure 22: Deep-Level I and Level II Depth map for Prospect Level I and II

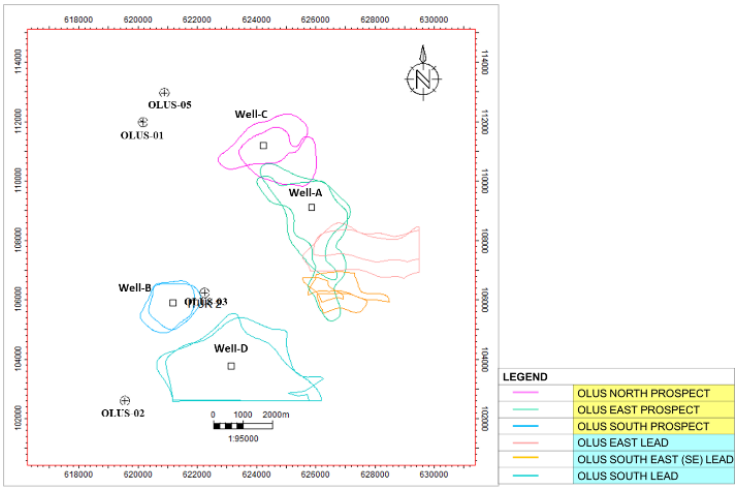

Figure 23: Prospect and Lead Map of OLUS Field

4Reservoirs Estimation of the Leads and Prospects within the OLUS field

OLUS EAST LEAD

As shown in Table 4 below, the OLUS East lead consists of two mid-level closures known as Mid-Level I and II. Mid-Level I has a GRV of 59,321.9 acre-ft, NTG of 0.81, porosity of 0.37, and water saturation of 0.45, as shown in the table, producing an Unrisked STOIIP of 68.96 MMBO with a POS of 0.20, which results in a Risked STOIIP of 13.79 MMBO. Mid-Level II is significantly larger but exhibits similar reservoir quality metrics, with an Unrisked STOIIP of 156.19 MMBO and a Risked STOIIP of 31.24 MMBO. Combining both mid-levels, the OLUS East lead exhibits a substantial unrisked inventory of approximately 225.16 MMBO and a risked inventory of 45.03 MMBO driven by high NTG, average porosity and water saturation as shown in the table.

OLUS SOUTH-EAST (SE) LEAD

The SE lead is a smaller and shallower play with Mid-Level I producing an Unrisked STOIIP of 4.86 MMBO and a Risked of 0.97 MMBO after POS, while the Mid-Level II is larger, producing an Unrisked of 41.63 MMBO and a Risked of 8.33 MMBO, as shown in Table 4 below. The combined SE lead unrisked is approximately 46.49 MMBO with a risked of 9.30 MMBO. Although smaller in absolute volume than OLUS East, the SE lead benefits from the same favourable petrophysical quality with high NTG and porosity, which yields relatively high recovery potential per unit area.

OLUS SOUTH LEAD

The South lead dominates the lead inventory numerically with Deep-Level I show an enormous GRV of 646,451 acres, combined with a very high NTG of 0.95, but lower and higher water saturations (from shallow level). Unrisked STOIIP values are significant, as shown in Table 4, but POS is low at 0.15, resulting in a risked STOIIP of approximately 65.97 MMBO. Deep-Level II is similar in scale, with unrisked STOIIP of approximately 439.94 MMBO and risked of 65.99 MMBO. Overall, the South lead exhibits an unrisked inventory of approximately 879.74 MMBO and a substantial risked inventory of 131.96 MMBO. The presence of very large GRV and exceptionally high NTG drives significant OOIP, despite modest porosity, while the low POS indicates deep-target uncertainties.

Table 4: Resource Estimation for leads within the OLUS field

Reservoir	GRV (Acre-ft)	Area (Acres)	NTG (frac)	Sw (frac)	Ø (frac)	OOIP (MMBO)	Bo	Unrisked STOIIP	POS	Risked STOIIP
OLUS EAST LEAD										
MID LEVEL I	59321.9	702.3139	0.81	0.45	0.37	75.86025	1.1	68.96386	0.2	13.79277
MID LEVEL II	146568	1256.489	0.81	0.45	0.37	187.4297	1.2	156.1914	0.2	31.23828
TOTAL								**225.1553**		**45.03105**
OLUS SOUTH-EAST (SE) LEAD										
MID LEVEL I	4182.95	132.4788	0.81	0.45	0.37	5.349114	1.1	4.862831	0.2	0.972566
MID LEVEL II	39065	506.43	0.81	0.45	0.37	49.95593	1.2	41.62994	0.2	8.325988
TOTAL								**46.49277**		**9.298554**
OLUS SOUTH LEAD										
DEEP LEVEL I	646451	2432.242	0.95	0.52	0.25	571.729	1.3	439.7916	0.15	65.96873
DEEP LEVEL II	696419	2380.313	0.95	0.52	0.25	615.9213	1.4	439.9438	0.15	65.99157
TOTAL								**879.7354**		**131.9603**

OLUS NORTH PROSPECT

The OLUS North prospects include two mid-level prospects with similar GRV and petrophysical parameters. Mid-Level I has a GRV of 38,643.3 acre-ft, and Mid-Level II has a GRV of 39,564.3 acre-ft. Both have an NTG of 0.81, porosity of 0.37, and water saturation of 0.45 as shown in Table 5 below. The unrisked STOIIP values are approximately 44.92 MMBO and 42.16 MMBO, respectively, resulting in a combined unrisked STOIIP of 87.09 MMBO and a risked STOIIP of 17.42 MMBO. As prospects, OLUS North demonstrates moderate-sized, technically consistent closures with good reservoir quality and moderate risk.

OLUS SOUTH PROSPECT

Table 5 presents OLUS South prospect as a deeper and smaller closure compared to the South lead, with Deep-Level I GRV of 38,805.2 acre-ft and Deep-Level II GRV of 20,492.8 acre-ft, with NTG at 0.95, porosity at 0.25, and water saturation of 0.52. Unrisked STOIIP totals approximately 39.35 MMBO, while Risked STOIIP is 5.90 MMBO, as shown in Table 5. However, despite high NTG, lower porosity, and higher water saturation at depth, which reduce STOIIP, the low POS indicates that deep targets pose risks.

OLUS EAST PROSPECT

The OLUS East prospect is a large deep play with Deep-Level I and Deep-Level II values, as shown in Table 5 below. Both levels have Unrisked STOIIP values of approximately 66.18 MMBO and 66.49 MMBO, respectively, resulting in a combined Unrisked STOIIP of about 132.67 MMBO and a Risked STOIIP of 19.90 MMBO. The East prospect has significant unrisked volumes due to its large areal extent and very high NTG, but lower porosity and deeper burial reduce volumetric efficiency and increase technical risk; POS reflects concerns about charge and seal.

Table 5: Resource Estimation for the Prospect within the OLUS field

Reservoir	**GRV (Acre-ft)**	**Area (Acres)**	**NTG (frac)**	**Sw (frac)**	**(frac)**	**OOIP (MMBO)**	**Bo**	**Unrisked STOIIP**	**POS**	**Risked STOIIP**
OLUS NORTH PROSPECT										
MID LEVEL I	38643.30	897.13	0.81	0.45	0.37	49.42	1.1	44.92	0.20	8.98
MID LEVEL II	39564.30	827.37	0.81	0.45	0.37	50.59	1.2	42.16	0.20	8.43
TOTAL								**87.09**		**17.42**
OLUS SOUTH PROSPECT										
DEEP LEVEL I	38805.20	926.64	0.95	0.52	0.25	34.32	1.3	26.40	0.15	3.96
DEEP LEVEL II	20492.80	555.98	0.95	0.52	0.25	18.12	1.4	12.95	0.15	1.94
TOTAL								**39.35**		**5.90**
OLUS EAST PROSPECT										
DEEP LEVEL I	97271.50	1530.71	0.95	0.52	0.25	86.03	1.3	66.18	0.15	9.93
DEEP LEVEL II	105258.00	1376.42	0.95	0.52	0.25	93.09	1.4	66.49	0.15	9.97
TOTAL								**132.67**		**19.90**

Environment of Deposition

The Calabar Flank records a complex depositional history during the Cretaceous period, reflecting a progressive shift from continental to fully marine environments. As shown in Figure 24 below, the earliest deposits belong to the Awi Formation, laid down in fluvial and deltaic systems, characterized by conglomerates, sandstones, and shales. These sediments are both texturally and mineralogically immature, indicating short transport distances and deposition within a continental tectonic regime. As sea levels rose and tectonic reconfiguration

occurred, sedimentation shifted into shallow marine settings, exemplified by the Mfamosing Limestone, which is dominated by bioclastic textures, algal stromatolites, and oolitic grainstones/packstones, reflecting high-energy inner-neritic environments. Later deposition introduced shale units formed in nearshore to open marine settings, some of which indicated dysoxic conditions that preserved organic matter, making them potential marginal hydrocarbon source rocks. Palynofacies analyses further refine this interpretation, identifying holomarine assemblages indicative of inner-neritic deposition and mixed fluvio-marine assemblages suggesting littoral influence.

AGE	LITHOLOGY		DESCRIPTION
Recent Eocene -	Benin Formation		Loose sands, pebbly and arkosic
Maastrichtian L. Campanian -	Nkporo Shale		Dark grey, very fissile carbonaceous shale with gypsum bands and some calcareous nodules
Santonian	Santonian Deformation		Santonian deformational episode characterized by period of folding of pre-existing rocks and erosion and/or non deposition.
Coniacian	ODUKPANI GROUP	New Netim Marl	Dark grey massive marls intercalating with flaggy, calcareous grey shale with thalassinoides structures
Turonian		Ekenkpon Shale	Grey fissile shale with thin bands of calcareous nodules, limestone and mudstone units. Abundant shell fragments, keeled ammonite, juvenile
Cenomanian		Un-named Shale	Dark gray shale, highly fissile and separated by the upper shale unit by a regressive mudstone
Mid - Albian		Mfamosing Limestone	White to light grey limestone, stromatolitic at the base, with abundant fossils (gastropods, corals, shell fragments)
Neocomian - Aptian	Awi Formation		Reddish brown, coarse to medium grained arkosic sandstone. Pebbly at the base and exhibit fining upward succession in cycles, graded bedding.
Precambrian	Precambrian Basement Complex		Southeastern Basement Complex – Oban Massif composed predominantly of granite gneisses, granites and granodiorites.

Figure 24: showing a Stratigraphic chart of the Calabar Flank (Petters et al., 2010)

The evolution of depositional environments within the Calabar Flank was strongly influenced by Cretaceous sea-level fluctuations and tectonic events, particularly faulting and the uplift of the Oban Massif, which governed accommodation space and sediment supply. The regional stratigraphic pattern, consistent with the transgressive model described by Kendall and Pomar (2005), shown in Figure 25 and supported by log motifs from the OLUS well, as shown in Figure 7, demonstrates an upward-deepening sequence from fluvial/deltaic to nearshore and shelfal systems. While not all sand bodies in the field are well developed, the most prominent log motifs provide a basis for interpreting potential reservoir intervals. For a more precise reconstruction of depositional facies and to assess lateral continuity of reservoir-quality sands, biostratigraphic studies, core analysis, and the integration of data from additional wells are recommended.

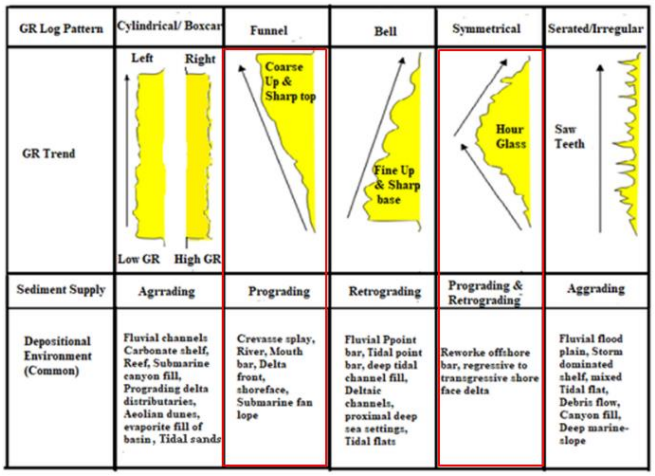

Figure 25: stratal stacking patterns using the gamma-ray logs (Kendrall & Pomar, 2005)

Discussion

The petrophysical analysis of the wells studied in the OLUS Field evaluated reservoir quality and hydrocarbon prospects in the field. The reservoirs, especially Sand B, display high net-to-gross ratios up to 0.95, indicating widespread clean sand bodies with minor shale between them. As shown in Table 2, average porosity readings across the sections reflect that pore systems can be suitable for hydrocarbon storage. The comparison of moderate to low water saturation and high hydrocarbon saturation confirms effective hydrocarbon trapping, as shown in Table 2. While low bulk volume of water (BVW) in most sands suggests minimal irreducible water saturation and a high likelihood of high productivity. Additionally, the repeated identification of oil-down-to (ODT) contacts across multiple wells supports the hypothesis of continuous hydrocarbon accumulation across the area. Overall, these results show that integrated petrophysical evaluation is effective in identifying productive zones and assessing the reservoir's commercial potential in the Calabar Flank of the Lower Benue Trough.

Moreover, the seismic interpretation of the OLUS Field delineates a structurally complex system that dominates across the study area. Time and depth mapping of Sand A and Sand B, together with mid- and deep-level horizons, revealed multiple closures with varying degrees of structural relief and amplitude support, indicating a mix of prospects and leads. RMS amplitude extraction over the prospect and lead areas shows that the amplitudes are consistent with the structure, which further increases the chance of success for the evaluated opportunities.

Furthermore, resource assessment of the OLUS Field reveals significant in-place hydrocarbons in both mid- and deep-level targets, as shown in Tables 4 and 5. Table 4 shows that OLUS East lead holds the largest mid-level unrisked STOIIP of 156.2 due to high NTG and porosity, while OLUS South dominates deep volumes from its large GRV despite poorer reservoir quality (Table 4). Low POS values, driven by trap and charge uncertainties, limit risked volumes in leads. Prospects show smaller but more certain volumes, with OLUS North offering balanced mid-level potential and OLUS East prospect showing deep upside (table 5). Overall, deep leads carry high volumes but greater risk. In contrast, prospects offer nearer-term, lower-risk drilling opportunities, highlighting the need to prioritise targets with favourable seismic, petrophysical, and structural attributes.

The depositional evolution of the Calabar Flank, as shown in the OLUS Field records, is a Cretaceous transgressive sequence that transitions from fluvial-deltaic systems of the Awi Formation to shallow marine carbonate platforms of the Mfamosing Limestone, and ultimately to nearshore-to-open marine shales. Palynofacies analyses further confirm alternating marine and fluvio-marine influences, consistent with shoreline migration caused by fluctuating sea levels and tectonic activity from the uplifted Oban Massif. This environmental framework directly impacts reservoir distribution, as high-energy fluvial and nearshore deposits primarily form the main sandstone reservoirs, while marine carbonates and shales act as both seal and, in some cases, source rocks. The interaction of tectonics, sea-level fluctuations, and sediment supply has resulted in laterally variable reservoir bodies, explaining the heterogeneity observed in seismic amplitude and petrophysical quality across the field. Understanding this depositional context is crucial for predicting reservoir continuity and quality, particularly when correlating seismic facies with well-log signatures during exploration and development planning.

Conclusions

The integrated petrophysical analysis of wells in the OLUS Field confirms the presence of high-quality reservoirs with net-to-gross ratios, excellent porosity, and favourable hydrocarbon saturations. Sand A and Sand B demonstrate strong reservoir potential with low bulk volume water and oil-down-to contacts, suggesting continuous hydrocarbon columns. These findings establish a solid reservoir framework and provide reliable parameters for volumetric estimation, while also highlighting zones with the best potential for commercial development. Additionally, the seismic data interpretation delineates a structurally complex petroleum system characterized by fault-bounded closures and other structural traps for hydrocarbons. Time and depth structure maps reveal several leads and prospects with varying degrees of structural relief and amplitude support. The mapping of mid-level and deep-level horizons reveals multiple play fairways, with amplitude anomalies often coinciding with structural highs, suggesting potential direct hydrocarbon indicators.

Furthermore, the resource estimation confirms significant unrisked STOIIP volumes across the OLUS Field, especially in deep-level leads such as OLUS South, driven by large GRVs and high NTG values despite moderate porosity and higher water saturations. Prospects at mid-levels, such as OLUS North and OLUS East, offer smaller but lower-risk opportunities with favourable reservoir quality. The depositional environment of the Calabar Flank, transitioning from continental fluvial-deltaic to shallow and open marine systems, has directly influenced the distribution, quality, and heterogeneity of the reservoirs. Understanding this, along with seismic and petrophysical results, supports the identification of priority drilling targets and underpins a strategic exploration plan that balances high-volume deep plays with lower-risk, high-quality mid-level prospects.

References

Adeleye, D. R., & Fayose, F. A. (1978). Stratigraphy of the type section of Awi Formation, Odukpani area, Southern Nigeria. *J Min Geol*, *15*, 33-57.

Ahmad, N., Khan, S., & Al-Shuhail, A. (2021). Seismic Data Interpretation and Petrophysical Analysis of Kabirwala Area Tola (01) Well, Central Indus Basin, Pakistan. *Applied Sciences*, *11*(7), 2911. https://doi.org/10.3390/app11072911

Aka MU, Effiong CI, Akpan DN (2022) Assessment of Nkporo Shales in Calabar Flank to Ascertain its Hydrocarbon Potentials, SouthSouth, Nigeria. J Geol Geophys. 11: 1027.

Al-Baldawi B. A. (2014). Petrophysical evaluation study of Khasib Formation in Amara oil field, South Eastern Iraq. *Arabian Journal of Geosciences*, *8*(4), 2051–2059. https://doi.org/10.1007/s12517-014-1371-5

Anyiam, O. A., Andrew, P. J., and Ikenna Christopher Okwara. (2017). Assessment of the heterogeneity and petrophysical evaluation of reservoirs in the "Akbar Field", Niger Delta, Nigeria. *Journal of Petroleum Exploration and Production Technology*, *7*(4), 1035–1050. https://doi.org/10.1007/s13202-017-0361-z

Boboye, O. A., and Okon, E. E. (2014). Sedimentological and geochemical characterization of the Cretaceous strata of Calabar Flank, southeastern Nigeria. *Journal of African Earth Sciences*, *99*, 427–441. https://doi.org/10.1016/j.jafrearsci.2014.04.035

Cook, M. (2021). Exploration. *Developments in Petroleum Science*, 69–100. https://doi.org/10.1016/b978-0-12-821190-8.00004-6

d'Almeida, G. A. F., Kaki, C., and Adeoye, J. A. (2016). Benin and Western Nigeria Offshore Basins: A Stratigraphic Nomenclature Comparison. *International Journal of Geosciences*, *07*(02), 177–188. https://doi.org/10.4236/ijg.2016.72014

Edet, J.J. and Nyong, E.E., (1993). Depositional environments, sea level history and paleobiogeography of the Late Campanian to Maastrichtian on the Calabar Flank, S.E. Nigeria. Paleoclimatology, Paleoecology, Vol. 102, pp 161 – 175.

Ekop, I. R., Bassey, C. E., Udoh, A. C., and Ekefre, A. E. (2025). Petrophysical Evaluation of Reservoir Properties Using Well Logs and 3D Seismic Data: A Case Study of the 'Northern' Field, Niger Delta. *Researchers Journal of Science and Technology*, *5*(3), 1–21. Retrieved from https://www.rejost.com.ng/index.php/home/article/view/176

Ekpo, B. O., Essien, N., Fubara, E. P., Ibok, U. J., Ukpabio, E. J., and Wehner, H. (2013). Petroleum geochemistry of Cretaceous outcrops from the Calabar Flank, southeastern Nigeria. *Marine and Petroleum Geology*, *48*, 171–185. https://doi.org/ 10.1016/ j.marpetgeo.2013.08.011

Ekwok, S. E., Akpan, A. E., and Ebong, E. D. (2021). Assessment of crustal structures by gravity and magnetic methods in the Calabar Flank and adjoining areas of Southeastern Nigeria—a case study. *Arabian Journal of Geosciences*, *14*(4). https://doi.org/10.1007/s12517-021-06696-1

Essien, N.U., Ukpabio, E.J., Nyong, E.E., and Ibe, K.A., 2005. Preliminary organic geochemical appraisal of Cretaceous rock unit in the Calabar Flank, Southern Nigeria. Journal of Mining and Geology, Vol. 41 (2), pp 181 – 191.

Falade, A. O., Amigun, J. O., and Abiola, O. (2024). Hydrocarbon prospective study using seismic inversion and rock physics in an offshore field, Niger Delta. *Discover Geoscience*, *2*(1). https://doi.org/10.1007/s44288-024-00030-4

Harry, T. A., Etim, I. U., and Etim, C. E. (2022). Sedimentology And Palynology Models Of Sedimentary Sections Along Lemna Section Of The Benin Formation, Cross River-Southern Nigeria. *Pakistan Journal of Geology (PJG)*, *6*(1), 24-28.

Hussein, I. A., Abu-Hashish, M., and El-Maadawy, K. (2024). Petrophysical evaluation and hydrocarbon potentiality of the Kareem sand reservoir at GS277 oil field, Gulf of Suez, Egypt. *Scientific Journal of Faculty of Science, Menoufia University*, *28*(1), 38–52. https://doi.org/10.21608/sjfsmu.2024.357488

Ilori, A. O. (2016). Occurrence of shale soils along the Calabar-Itu highway, Southeastern Nigeria and their implication for the subgrade construction. *SpringerPlus*, *5*(1). https://doi.org/10.1186/s40064-016-1822-4

Kendall, C.G. and Pomar, L. (2005). System tract bounding surfaces, lithofacies, geometric hierarchies and stacking patterns: Keys to shallow watercarbonate interpretation. AAPG Bull., v.89.

Khan, Z. U., Ahmed, Z., Naseer, M. T., Kontakiotis, G., Naseem, S., Hammad Tariq Janjuhah, A. A., and Panagiotopoulos, I. P. (2024). Assessing the hydrocarbon potential of the Kadanwari gas field using integrated seismic and petrophysical data. *Journal of Petroleum Exploration and Production Technology*, *14*(6), 1349–1364. https://doi.org/10.1007/s13202-024-01780-0

Mheluka, J. M., and Mulibo, G. D. (2018). Petrophysical Analysis of the Mpera well in the Exploration Block 7, Offshore Tanzania: Implication on Hydrocarbon Reservoir Rock Potential. *Open Journal of Geology*, *08*(08), 803–818. https://doi.org/ 10.4236/ ojg.2018.88047

Murat, R.C., (1972). Stratigraphy and paleogeography of the Cretaceous and Lower Tertiary in Southern Nigeria. In: T. J. Dessuavagie (Ed.), African Geology (251- 266). Ibadan: University Press.

Nton, M. E., Akpan, O. S., and Adamolekun, O. J. (2018). Geochemistry of Ekenkpon and Nkporo shales, Calabar flank, SE Nigeria: implications for provenance, transportation history and depositional environment. *Global Journal of Geological Sciences*, *16*(1), 63–63. https://doi.org/10.4314/gjgs.v16i1.7

Nwaezeapu, V. C., Ezenwaka, K. C., and Ede, T. A. (2019). Evaluation of hydrocarbon reserves using integrated petrophysical analysis and seismic interpretation: A case study of TIM field at southwestern offshore Niger Delta oil Province, Nigeria. *Egyptian Journal of Petroleum*, *28*(3), 273–280. https://doi.org/10.1016/j.ejpe.2019.06.002

Nwaezeapu, V. C., Ezenwaka, K. C., and Ede, T. A. (2019). Evaluation of hydrocarbon reserves using integrated petrophysical analysis and seismic interpretation: A case study of TIM field at southwestern offshore Niger Delta oil Province, Nigeria. *Egyptian Journal of Petroleum*, *28*(3), 273–280. https://doi.org/10.1016/j.ejpe.2019.06.002

Nyong, E.E., and Ramanathan, R.M., (1985). A record of oxygen-deficient paleoenvironments in the Cretaceous of the Calabar Flank, SE Nigeria. J. Afr. Earth Sc. 3 (4), 455–460.

Odumodu, C. F. (2012). Temperatures and Geothermal gradient fields in the Calabar Flank and parts of the Niger Delta, Nigeria. *Petroleum Technology Development Journal*, *2*(2), 1-15.

Ogidi, A. O., Essien, N. U., Okon, E. E., Nton, M. E., and A, J. C. (2021). Evaluation of the Shale Gas Potentials of Ekenkpon Shale, Calabar Flank, Southeastern Nigeria. *NAPE Bulletin*, *30*(1), 55–69. https://www.researchgate.net/publication/357854115_Evaluation_of_the_Shale_Gas_Potentials_of_Ekenkpon_Shale_Calabar_Flank_Southeastern_Nigeria

Okiwelu, A., Okwueze, C., Okereke, C. S., and Osazuwa, I. (2010). Crustal structure and tectonics of the Calabar Flank, West Africa, based on residual gravity interpretation. *European journal of scientific research*, *42*(2), 195-203.

Okon, E. E., and Ojong, R. A. (2019). Paleoenvironmental analysis and its significance in sedimentology: case study of the conglomerate facies of the Awi Formation, Calabar Flank, Southeast Nigeria. *Advances and trends in physical science research*, *2*.

Oluwajana, O. A., and Ehinola, O. A. (2018). Potential shale resource plays in southeastern Nigeria: petroleum system modelling and microfabric perspectives. *Journal of African Earth Sciences*, *138*, 247-257.

Omigie J.I., and Alaminiokuma G.I. (2020). Petrophysical Evaluation of Reservoirs for Hydrocarbon Reserve Estimation in Eastern Central Swamp Depobelt, Niger Delta. Malaysian Journal of Geosciences, 4(2): 57- 63.

Onita, F. B., Ebeh, C. O., and Iriogbe, H. O. (2023). Advancing Quantitative Interpretation Petrophysics: Integrating Seismic Petrophysics for Enhanced Subsurface Characterization. *Engineering Science & Technology Journal*, *4*(6), 617–636. https://doi.org/ 10.51594 /estj.v4i6.1446

Oyeyemi, K. D., Olowokere, M. T., and Aizebeokhai, A. P. (2017). Hydrocarbon resource evaluation using combined petrophysical analysis and seismically derived reservoir characterization, offshore Niger Delta. *Journal of Petroleum Exploration and Production Technology*, *8*(1), 99–115. https://doi.org/10.1007/s13202-017-0391-6

Paul, S. S., Okwueze E. E., and Udo, K. I. (2018). Petrophysical Analysis of Well Logs for the Estimation of Oil Reserves in Southern Niger Delta. *International Journal of Advanced Geosciences*, *6*(1), 145–145. https://doi.org/10.14419/ijag.v6i1.11815

Petters S. W., Nyong E. E., Akpan E. B., and Essien N. U. (1995). Lithostratigraphic revision for the Calabar Flank, S. E. Nigeria. Proceedings of the 31st Anniversary conference of Nigeria Mining and Geosciences Society, Calabar

Petters, S. W., Zaborski, P.MP., Essien, N. U., Nwokocha, K. D., and Inyang, D.O., (2010). Geological excursion guidebook to the Cretaceous of the Calabar Flank, Southeast Nigeria. Nigerian Mining and Geosciences Society 46th Annual Conference "Calabar 2010". Shamber Grafitech Studio. 28p.

Petters, S.W., (1982). Central West Africa Cretaceous – Tertiary benthic foraminifera and stratigraphy. Paleontogr. 179A, 1–104.

Ramanathan, R.M., and Kumaran, K.P.N., (1981). Age and paleoecology of M-1 well in the Calabar Flank, southeastern Nigeria. J. Mining Geol. 18, 163–171.

Reijers T. J. A. (1998). The Mfamosing Limestone In Se Nigeria: Outcrop-Subsurface Correlation And Reservoir Development. *Journal of Petroleum Geology*, *21*(4), 467–481. https://doi.org/10.1111/j.1747-5457.1998.tb00796.x

Reijers T. J. A., and Petters, S. W. (1987). Depositional Environments And Diagenesis Of Albian Carbonates On The Calabar Flank, Se Nigeria. *Journal of Petroleum Geology*, *10*(3), 283–294. https://doi.org/10.1111/j.1747-5457.1987.tb00947

Reyment, R.A., (1965). Aspects of the Geology of Nigeria, Ibadan University Press, Ibadan, 143pp.

Saadu, Y. K., and Nwankwo, C. N. (2018). Petrophysical evaluation and volumetric estimation within Central swamp depobelt, Niger Delta, using 3-D seismic and well logs. *Egyptian Journal of Petroleum*, *27*(4), 531–539. https://doi.org/10.1016/j.ejpe.2017.08.004

Selema, S. B., Ideozu, R. U., and Acra, E. J. (2023). Mid Cretaceous Subsurface Carbonate Deposit And Reservoir Development Of The Mfamosing Limestone *Calabar Flank. International Journal of Research -GRANTHAALAYAH, 11(5), 112–128. https://doi.org/* 10.29121/ granthaalayah.v11.i5.2023.5175

Udo, I. G., Udofia, P. A., Etukudo, N. J., and Adesina, D. A. (2023). Paleoenvironmental interpretation of the exposed section of the Benin Formation in southeastern part of the Niger Delta Basin, Nigeria: A pebble morphometric approach. *IOSR Journal of Applied Geology and Geophysics*, *11*, 12-19.

Ukpong, A. J., Ekhalialu, O. M., Ogidi, A. O., and Osung, W. E. (2017). Provenance and Depositional Environment of Sediments of the Awi Formation, Calabar Flank, Southeastern Nigeria.